Journal of Energy Storage 21 (2019) 519–527

Contents lists available at ScienceDirect

Journal of Energy Storage

journal homepage: www.elsevier.com/locate/est

Aging characterization and modeling of nickel-manganese-cobalt lithium-ion batteries for 48V mild hybrid electric vehicle applications

Zifan Liu[a], Andrej Ivanco[a], Simona Onori[b,*]

[a] Automotive Engineering Department, Clemson University, Greenville, SC, 29607 USA
[b] Energy Resources Engineering Department, Stanford University, USA

ARTICLE INFO

Keywords:
Lithium-ion battery
48V mild hybrid
Modeling

ABSTRACT

This paper investigates the cycle aging behavior of nickel-manganese-cobalt (NMC) lithium ion battery cells under high current rates and narrow window of State-of-Charge (SOC) variation for 48 V mild hybrid electric vehicle (HEV) applications. The charge sustaining aging profiles were synthesized from real-world duty cycles in some of the authors' previous work [44,45] and used in the laboratory for life cycle aging testing spaced out by periodic cell capacity tests performed to assess cell aging conditions. Furthermore, at each 1C discharged aging characterization stage, the parameters of a physics-based electrochemical cell model were identified using the Bayesian Markov Chain Monte Carlo (MCMC) method. Among the parameters that can be identified with sufficient accuracy from the experimental data, the concentration of lithium-ions at the negative electrode after full charge is found to be strongly correlated with the system-level loss of capacity. These results provide new insights on the aging performance of NMC lithium ion cells in battery management system for 48 V hybrid vehicles.

1. Introduction

Hybrid electric vehicles (HEVs), plug-in hybrid electric vehicles (PHEVs) and battery electric vehicles (BEVs) are being widely deployed to improve powertrain fuel efficiency and reduce tailpipe emissions. Their market acceptance demands refined battery technologies in terms of lifetime, safety, specific energy, specific power and cost. The lithium-ion chemistry is gaining popularity and expanding dominance into electric vehicles. However, to fulfill customer expectations with respect to electric range and service life across real-world usage, manufactures have often chosen to oversize the lithium ion battery pack in sacrifice of costs. Therefore, efficient management and optimized design along with deeper understandings on lithium ion battery aging have been the main research foci to minimize ownership costs [1].

It is common to separate lithium ion battery aging processes by calendar aging under storage and cycle aging upon usage. While calendar aging is stressed by time, temperature and State of Charge (SOC), cycle aging introduces additional stressors such as Ampere-hour (Ah) throughput, SOC change (ΔSOC), and current rate. To understand the impacts from these aging stressors, well-controlled test activities are usually conducted in laboratory. Previous testing efforts have been reported for lithium ion chemistries with different positive electrode materials, such as, lithium nickel-manganese-cobalt (NMC) [2–8], lithium manganese oxide (LMO) [9,10], lithium NMC-LMO composite [11–14], lithium iron-phosphate (LFP) [15–18], and lithium nickel-cobalt-aluminum (NCA) [19,20]. This study focuses on the cycle aging performance of NMC cells in a 48 V system. The test matrices used in previous studies [2–7] combine different ΔSOCs around different SOCs and at 1C discharge/charge rate with fixed temperatures. In [8], on the other hand, an extended design of experiment comprises 5 ΔSOCs, 3 charging rates (0.2C, 0.5C, 1C), 3 discharge rates (0.5C, 1C, 2C) and 3 temperatures (25 °C, 35 °C, 50 °C) at 50% SOC. Given the low current rate ($\leq$2C) and wide ΔSOCs, these experiments were mainly designed for high energy applications such as BEV and PHEV. A gap clearly exists in the understandings of NMC cell aging performance in HEV applications with high current rates and narrow state of charge excursion (compatible with a ΔSOC in the range of 15–30%) for charge sustaining operation.

The aging of lithium-ion battery cells manifests as capacity loss and resistance growth [21,22]. Aging models are regarded as useful tools to interpret aging test results and predict cell performance. While data-driven (see [23,24],) and empirical (see [2,7,25–31,42],) aging models view the cell as a whole entity, physics-based aging models offer an alternative perspective to look into the cell at the electrode or even finer levels. The basis for the construction of physics-based aging models is the physics-based electrochemical cell model which describes

* Corresponding author.
E-mail addresses: zifanl@clemson.edu (Z. Liu), aivanco@clemson.edu (A. Ivanco), sonori@stanford.edu (S. Onori).

https://doi.org/10.1016/j.est.2018.11.016
Received 30 September 2018; Received in revised form 2 November 2018; Accepted 15 November 2018

the fresh cell dynamics [32–41]. In some studies [33,39], the electrochemical cell models are extended to aging models by adding the governing equations of aging reactions; in other studies [35,41], a subset of parameters of the electrochemical cell model are updated according to empirical relations to account for aging effects. This study adopts the single particle (SP) electrochemical cell model for the aging investigation [33–35].

However, one challenge of using the electrochemical cell model lies in the identification of multiple model parameters. It is common practice to regard the parameter identification problem as a nonlinear optimization problem, aimed at minimizing the least-square difference between model outputs and experiment measurements. Several numerical algorithms are available and have been successfully applied for this nonlinear optimization problem. They can be categorized as gradient-based algorithms, such as Levenberg-Marquardt method [35], trust region algorithm [36], and Newton method [41]; and non-gradient-based algorithms, such as genetic algorithm [38], simplex search method [40], and particle swarm optimization algorithm [40]. While the results of gradient-based algorithm can be easily trapped in local minima, the non-gradient-based algorithms have the potential to converge to the global minima or maxima from any initial values.

Additionally, experimental data might fail to provide the information needed to carry out full parameter set identification. In this regard, the single-factored sensitivity analysis can generally be used as the base line study to assess the dependence of the model output on each parameter as done in [36], where different aging scenarios were tested to identify aging parameters of an electrochemical model for the 26650 Lithium-ion battery cells based on iron-phosphate chemistry.

This approach, though, only gives local sensitivity results when applied to nonlinear models. To gain more insights about the ability to identify model parameters from output measurements, the Fisher information method can be used, as in [37,40], where single-factored sensitivity analysis study and covariance matrix evaluation from measurements were combined in a unified approach. Nevertheless, the potential interaction among all parameters is not taken into account. In [41], a Markov Chain Monte Carlo (MCMC) method was proposed to stochastically estimate the parameter distributions. The effective parameters and their uncertainties are estimated using a reformulation and simplification of the pseudo-two-dimensional (P2D) model from [32] for offline application. The cell chemistry and type, along with the specific battery application used in [41] were not reported, leaving the applicability and generalization of the results debatable.

In this paper, we identify and validate a single particle (SP) electrochemical model using data collected on 18650 NMC lithium-ion batteries to mimic the behavior of a 48 V HEV battery. The MCMC-based method is used to carried out the parameter identification. The novel contribution of the paper is in the experimental aging campaign carried out for a micro hybrid battery application and the application of MCMC to identify the parameters of a SP model to predict the aging behavior of a 48 V battery.

The rest of this paper is organized as follows. Section II reports the experimental setup of the cycle aging tests along with test results. Section III details the SP electrochemical cell model, and in Section IV the MCMC algorithm used to identify the SP model parameters across aging is introduced and a discussion of the aging mechanisms occurring in the NMC cell tested using the customized test campaign is provided. Results and their relevance for the NMC cell aging performance in 48 V systems is summarized in Section V.

2. Experimental setup

In this study, aging experiments are conducted over cylindrical NMC 18650 lithium ion cells with rated capacity of 2 Ah (at 1C discharge rate) and nominal voltage of 3.6 V. Cell specifications are listed in Table 1. The aging test profiles were designed by synthesizing cell duty cycles experienced by a 48 V mild hybrid vehicle battery [43]. In particular, the duty cycles were categorized in terms of driving style (calm/normal/aggressive) and mean cycle speed (low/medium/high). They were synthesized for cell aging testing through a frequency analysis based on a power spectral density estimation approach [44]. The aging campaign consists of cycling NMC cells using the calm low (CLS) speed and the aggressive high speed (AHS) profiles, shown in Fig. 1 (a) and (b), at two different temperatures, i.e. 23 °C and 45 °C. The CLS and AHS driving cycles are a synthetic representation, in terms of mean speed and driving style, of a set of naturalistic vehicle drive cycles carried out using Welch's power spectral density approach [44]. The drive cycle data source used in [44] was obtained from the household travel survey from June 2001 to March 2002 conducted by SCAG (Southern California Association of Governments). The data were made publicly available through the U.S. Department of Energy's National Renewable Energy Laboratory (NREL) [49].

Table 1
NMC 18650 cell specifications.

Specifications	Unit	Values
Chemistry		Nickel-Manganese-Cobalt (NMC) Lithium ion
Nominal Capacity	Ah	2.0 (at 1C discharge)
Nominal Voltage	V	3.6
Max Discharge Continuous Current	A	32
Discharge Cutoff Voltage	V	2.5
Max Charge Continuous Current	A	12
Charge Cutoff Voltage	V	4.2
Internal Impedance	mΩ	12 (measured by AC 1 kHz)

For validation purposes, a new aging profile, shown in Fig. 1 (c), was designed and used in the experimental campaign. It was constructed by adding one micro charge profile to the aggressive high speed profile while using the shorter discharge time period from the calm low speed profile. In this way, the new condition accounts for an average discharge current of 16.1 A. Such a high current rate represents an accelerating stress factor in the context of hybrid vehicle applications. The temperature was fixed at 45 °C for the new validation profile. Moreover, for repeatability considerations, two cells (Cell#9 and Cell#10) were tested under this new condition. All aging profiles kept cycling the cells around 50% SOC to represent the typical HEV charge sustaining operating conditions.

Experiments were carried out in the Battery Aging and Characterization (BACh) Laboratory at the Automotive Engineering Department, Clemson University. The experimental setup used for the aging campaign, shown in Fig. 2, is composed of the Arbin BT-2000 battery cycler with a programmable power supply and an electronic load; a MITS Pro data acquisition software for the programming of test profiles and the control of the Arbin cycler; Peltier junctions that are in direct contact with the cell fixtures for thermoelectric temperature control. All cells underwent periodic capacity and internal resistance characterization tests at room temperature (~23 °C) throughout the aging campaign. The capacity test at 1C rate (2 A, nominal capacity value) consists of four steps: 1) charging the cell to 4.2 V at 1C constant current; 2) holding constant voltage at 4.2 V until the current drops to C/50; 3) 1 h rest; 4) discharging at 1C to the cut-off voltage of 2.5 V.

For calculation of the internal resistance, the hybrid pulse power characterization (HPPC) profile was executed [50]. The HPPC profile consists of an 18s 2C discharge pulse followed by a 40 s rest period and 10 s 1.5C charge pulse followed by a 40 s rest period. Each pulse is applied every 10% SOC decrease between 90% and 20% SOC. Both the capacity and HPPC tests profiles are depicted in Fig. 3. The 10 cells used in the aging campaign are listed in Table 2 based on their aging condition, e.g., CLS45 indicates a cell tested using the Calm Low Speed profile at 45 °C. Cells #7 and #8 were tested using the AHS45 profile for only 9 weeks due to the premature aging that occurred under the high-rate and high-temperature condition. Cells #9 and #10, tested under

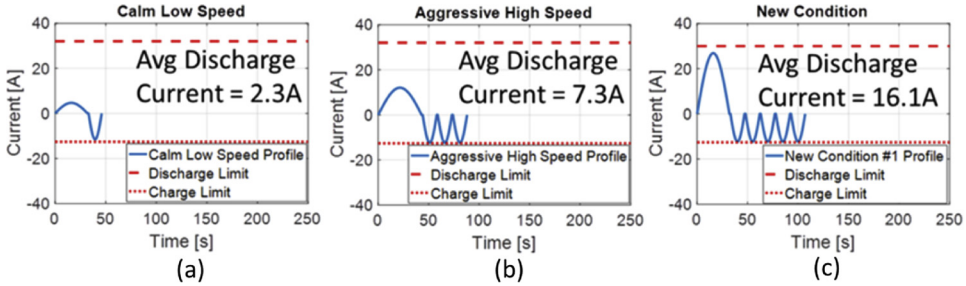

Fig. 1. Aging test profiles designed to represent different driver styles, (a) Calm Low Speed (CLS) profile, (b) Aggressive High Speed (AHS) profile, and (c) New Condition (NC) profile which is designed to validate the cycle aging performance of NMC lithium-ion cell.

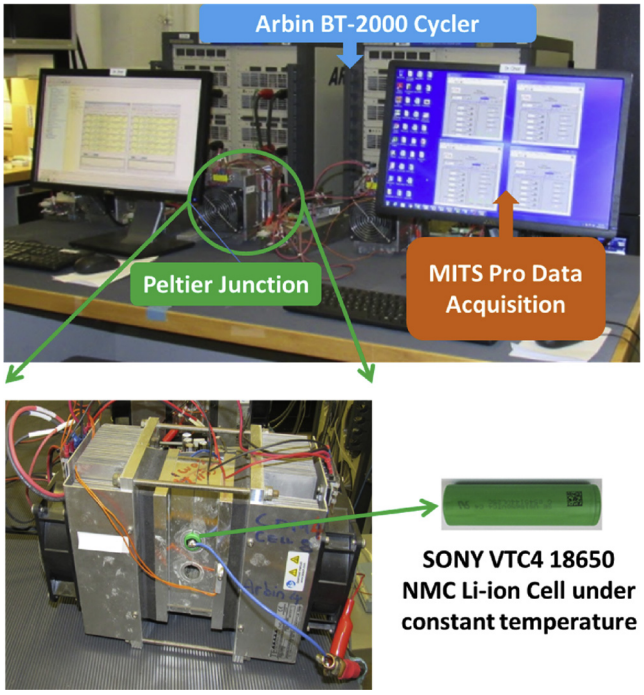

Fig. 2. Experimental test set-up at the BACh Laboratory. The Arbin BT-2000 cycler discharges and charges the cell continuously, according to the request from the interface of the MITS Pro data acquisition software. During testing, the Peltier junctions maintain the cell at a constant temperature.

the New Condition cycle and characterized by a higher C-rate than the AHS45 cycle, lasted for only 6 weeks. On the other hand, cells #1, #3 and #5 were cycled for 12 weeks whereas their 'sister' cells, #2, #4 and #6, tested under the same conditions, were terminated earlier than 12 weeks given that similar aging trends were observed. The normalized capacity losses are compiled in Fig. 4 (a), for the time-based aging and Fig. 4 (b), for kAh-throughput-based aging. For both scenarios, Cells #1 and #2 under CLS23 cycle show no capacity loss after 3-month of aging. Interestingly, for CLS45 Cell#3 and AHS23 Cell#6, capacity recoveries are observed during the first few aging characterization stages. The recovery in capacity is suggested to possibly be due to increased electrode active surface area, resulting from cracking of the positive electrode material grains [39,40]. But when compared to their repeated counterparts, those recoveries can be regarded as outliers. The observed capacity loss severity is in following order: the AHS45 and NC45 cases as the most severe, the CLS45 cases are next followed by the AHS23 cases, and, finally, the CLS23 cases. The aging results can be interpreted as: 1) the impact from temperature is larger than the impact on discharge current magnitude; 2) the impact from discharge current magnitude is larger at high temperature; 3) the impact from temperature is larger at higher discharge current rate.

When comparing the AHS45 cases and NC45 cases, in Fig. 4 (a), the test time compression can be observed since in the NC45 cases 10% capacity loss is achieved after only 6 weeks, whereas AHS45 cases need about 9 weeks. To understand the accelerating factors behind the time compression effect, both cases are further compared in Fig. 4 (b) which it shows that for AHS45 and NC45 cases, they actually achieve 10% capacity loss with almost equivalent Ah-throughput despite different discharge current rate.

Therefore, the time compression effect in Fig. 4 (a) is mainly attributed to more battery usage in terms of Ah-throughput, but not to more aggressive battery usage in terms of higher current rate. In other words, the impact from discharge current rate on battery aging is limited beyond the AHS45 cases in our aging campaign for the NMC lithium ion chemistry.

3. Single particle electrochemical cell model

In this section, a physics-based electrochemical model is introduced. While physical phenomena inside the cell are intrinsically due to microscale dynamics, reduced-complexity macro-scale models can be used to capture cell level dynamics. The pseudo-two-dimensional (P2D) model, firstly proposed in [32], uses nonlinear coupled partial differential equations to describe the mass diffusion and the potential distribution inside and between the porous electrodes and the electrolyte. A tradeoff between model fidelity and model complexity is achieved by simplifying the P2D model through approximation of each porous electrode as a single spherical particle. This results in either the single-particle (SP) model [33,35] or the enhanced single-particle (ESP) model [36,37]. The difference among these two models is that the latter includes the electrolyte dynamics that are not negligible in high current scenarios. In contrast, the SP model holds accuracy when used in low current rate applications ($\leq$1C). With 1C discharge capacity test data, this study pertains to the application of the physics-based SP model to execute the parameter identification algorithm.

The lithium ion battery can be simplified by representing each electrode as a spherical particle, as shown in Fig. 5. The lithium ions intercalate between two electrodes during discharging and charging. The intercalation resistance at the electrode surface exhibits in the form of overpotential. These phenomena can be described by the SP model through the following equations.

The concentration of lithium ions within the spherical particle at each electrode follows the Fick's diffusion law:

$$\frac{\partial c_i}{\partial t} - D_i \frac{1}{r_i^2}\frac{\partial}{\partial r_i}\left(r_i^2 \frac{\partial c}{\partial r_i}\right) = 0 \tag{1}$$

which is subject to boundary conditions:

$$D_i \frac{\partial c_i}{\partial r_i} = 0, \text{ at } r_i = 0 \text{ and for } t \geq 0 \tag{2}$$

$$D_i \frac{\partial c_i}{\partial r_i} = -j_i, \text{ at } r_i = R_i \text{ and for } t \geq 0 \tag{3}$$

where the subscript i= n is used for negative electrode, i= p is used for

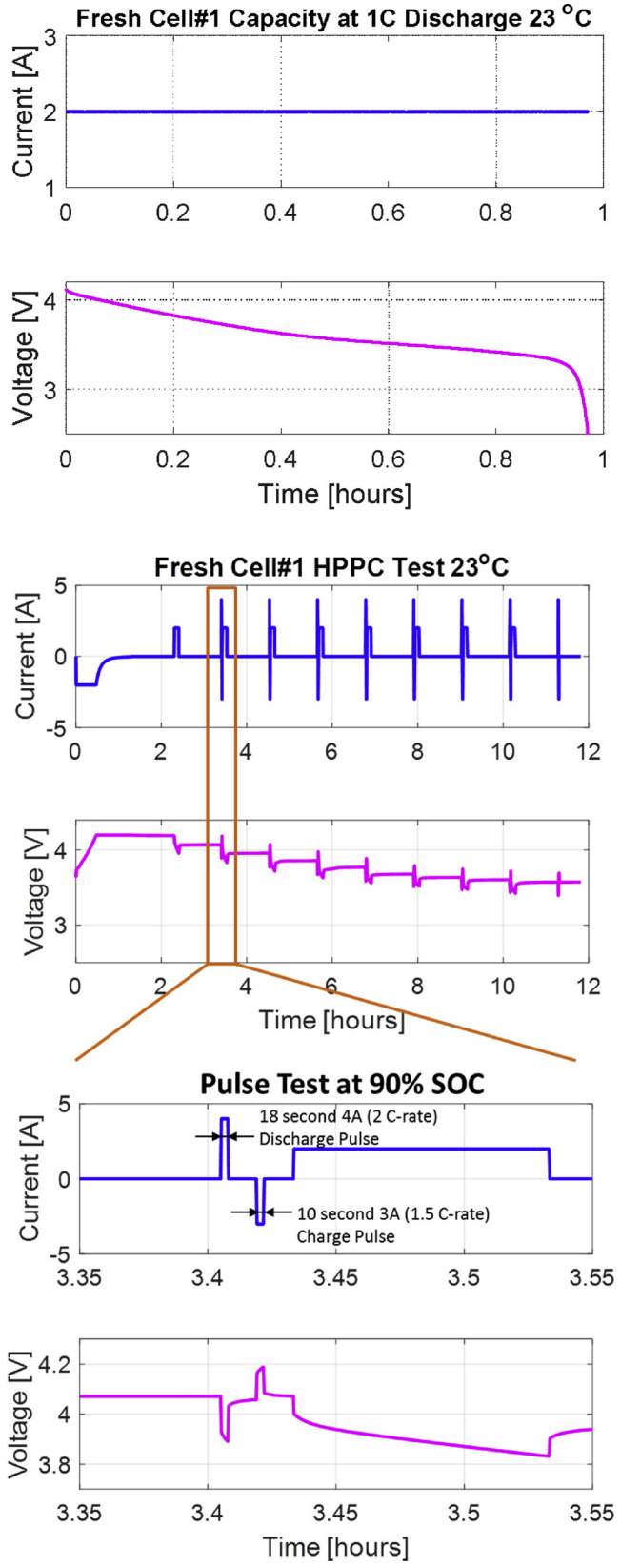

Fig. 3. The current and voltage responses for 1C discharge capacity test (top) and HPPC test (below) from fresh new cell#1. The discharge capacity test is done at 1C (or 2 A), the HPPC test profile consists of 2C (or 4 A) discharge pulse and 1.5C (or 3 A) charge pulse at every 10% SOC increment.

Table 2
The aging test matrix with the aging conditions and their corresponding cells.

Aging Conditions	Cell No. #
Calm Low Speed 23 °C (CLS23)	Cell#1 / Cell#2
Calm Low Speed 45 °C (CLS45)	Cell#3 / Cell#4
Aggressive High Speed 23 °C (AHS23)	Cell#5 / Cell#6
Aggressive High Speed 45 °C (AHS45)	Cell#7 / Cell#8
New Condition 45 °C (NC45)	Cell#9 / Cell#10

positive electrode; $c_i(r, t)$ is the solid-phase concentration (mol/m^3); D_i is the diffusion coefficient of the electrolyte in the solid particle (m^2/s); R_i is the radius of the solid particle (m); r_i is the distance from the center of the particle (m); t is the time instant (s); $j_i(t)$ is the lithium ion intercalation flux density (A/m^2), calculated as:

$$j_i(t) = \frac{I(t)}{A_i} \tag{4}$$

where I(t) is the applied current (A), positive for discharge, negative for charge and A_i is the equivalent electro-active surface area (m^2).

It is common practice to reduce the Eq. (1) into an ordinary differential equation by assuming a parabolic electrode lithium ion concentration profile [45]:

$$c_i(r_i,t) = a_i(t) + b_i(t)\frac{r_i^2}{R_i^2} \tag{5}$$

After substituting Eq. (5) into Eq. (1), one obtains:

$$\frac{d(a_i(t))}{dt} + \frac{r_i^2}{R_i^2}\frac{d(b_i(t))}{dt} = 6\frac{D_i b_i(t)}{R_i^2} \tag{6}$$

And after substituting Eq. (5) into Eq. (3), one obtains:

$$2\frac{D_i b_i(t)}{R_i} = -j_i(t) \tag{7}$$

Two quantities are of interests for the present study, i.e., the average concentration, $c_{avg,i}(t)$ and the surface lithium ion concentration, $c_{s,i}(t)$. The $c_{avg,i}(t)$ is calculated as:

$$c_{avg,i}(t) = \int_{r_i=0}^{R_i} 3\frac{r_i^2}{R_i^3} c_i(r_i,t)\,d(r_i) \tag{8}$$

which, after substituting Eq.(5) into Eq.(8), becomes:

$$c_{avg,i}(t) = a_i(t) + \frac{3}{5}b_i(t) \tag{9}$$

On the other hand, $c_{s,i}(t)$ is obtained by substituting $r_i = R_i$ into Eq. (5):

$$c_{s,i}(t) = a_i(t) + b_i(t) \tag{10}$$

Combining Eqs. (7), (9) and (10),

$$\frac{d}{dt}c_{avg,i} + 3\frac{j_i(t)}{R_i} = 0 \tag{11}$$

$$\frac{D_i}{R_i}(c_{s,i} - c_{avg,i}) = -\frac{j_i(t)}{5} \tag{12}$$

From $c_{avg,i}(t)$, one can determine the state-of-charge at the electrodes, $SOC_i(t)$, after normalizing $c_{avg,i}(t)$ with respect to the maximum electrode lithium ion concentration (mol/m^3), $c_{max,i}$:

$$SOC_i(t) = \frac{c_{avg,i}(t)}{c_{max,i}} \tag{13}$$

The electrode surface overpotentials, η_i (t), which are caused by the resistance of the flow of electrons at the electrode-electrolyte interface, can be calculated as:

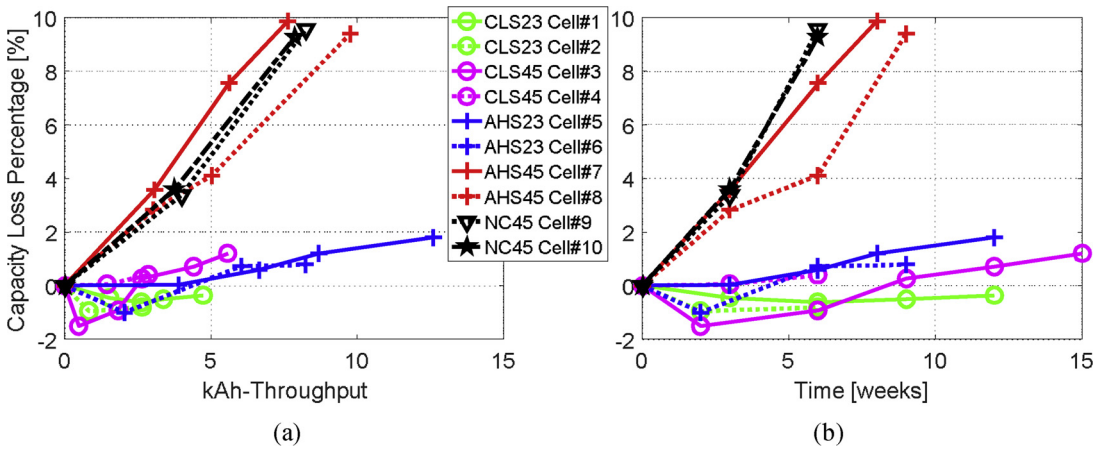

Fig. 4. The capacity loss in the aging campaign; (a) time-based, (b) kAh-throughput-based.

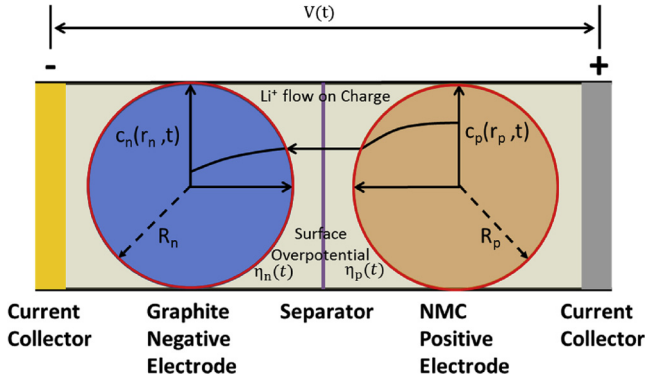

Fig. 5. Schematic of the electrochemical battery model using SP approximation.

$$\eta_i(t) = \frac{RT}{0.5F}\text{asinh}\left(\frac{j_i(t)}{2d_{0,i}(t)}\right) \tag{14}$$

where

$$d_{0,i}(t) = F\cdot k_i\cdot\sqrt{c_e(t)\cdot c_{s,i}(t)\cdot(c_{max,i} - c_{s,i}(t))} \tag{15}$$

represents the exchange current density (A/m^2); R is the universal gas constant, 8.314 J mol^{-1} K^{-1}; T is the temperature (K); F is the Faraday constant, 96487 (C/mol); k_i is the reaction rate constant ($m^{2.5}/mol^{0.5}/s$); $c_e(t)$ is the solution phase concentration (mol/m^3).

The cell voltage response output, $V_{output}(t)$, is determined by the open circuit potentials (OCP), $U_i(t)$ at the two electrodes, and the overpotentials, $\eta_i(t)$ of the two electrodes, and the contact resistance voltage drop, $R_f\cdot I(t)$. The OCP curves, $U_i(t)$, are shown in Fig. 6 where $SOC_i(t)$ is calculated according to Eq. (13).

$$V_{output}(t) = U_p(t) + \eta_p(t) - U_n(t) - \eta_n(t) - R_f\cdot I(t) \tag{16}$$

The SP electrochemical model described above introduces 14 parameters which are summarized in Table 3. The initial values are compiled from previous literature [25,38]. The coupling between k_i and c_e in the form of $k_i\sqrt{c_e}$ in Eq. (9) indicates that only 13 effective parameters should be identified. In this study c_e is always fixed at 1000 mol/m^3 to enable the effective identification of k_i. The inherent drawback of neglecting solution phase dynamics limits the application of single-particle model to the low current rate scenarios (usually less than 1C). In our case, the discharge capacity measurements (at 1C) are qualified for the adoption of SP model.

In the following section, the parameters of the SP electrochemical cell model are fitted at different aging stages. The identification algorithm is detailed in the next section. The parameters are identified in terms of their stochastic distributions and their correlations with cell-level aging quantities, such as capacity, are investigated.

4. Parameter identification with MCMC algorithm

In this study the MCMC algorithm is used to identify the stochastic distribution of the parameters of the SP cell model. The MCMC algorithm integrates the Bayesian stochastic-based feature, as it treats each parameter as a probabilistic distribution, with the stochasticity of Monte Carlo method, which uses sampling methods to approximate the parameter distributions [48]. The MCMC algorithm is applied to fit the parameters of the SP model with the 1C discharge capacity test data at different aging stages. The progression of the most significant aging-related parameters can provide new insights for NMC Li-ion battery aging. The application of the MCMC algorithm on the SP model for NMC aged cells operating for a 48 V system is proposed for the first time.

In the context of full discharge capacity test, in [38] it is indicated that $SOC_{n,100}$, $SOC_{p,100}$, A_p are the most significant parameters related to aging when the SP model is used; [41] evaluated the drift of the D_n, D_p, k_n k_p parameters during aging based on the P2D model. $SOC_{n,100}$, $SOC_{p,100}$, D_n, k_n are assumed to account for the resistive film growth at the negative electrode; A_p, D_p, k_p are mainly considered to account for active material losses at the positive electrode. Other parameters are

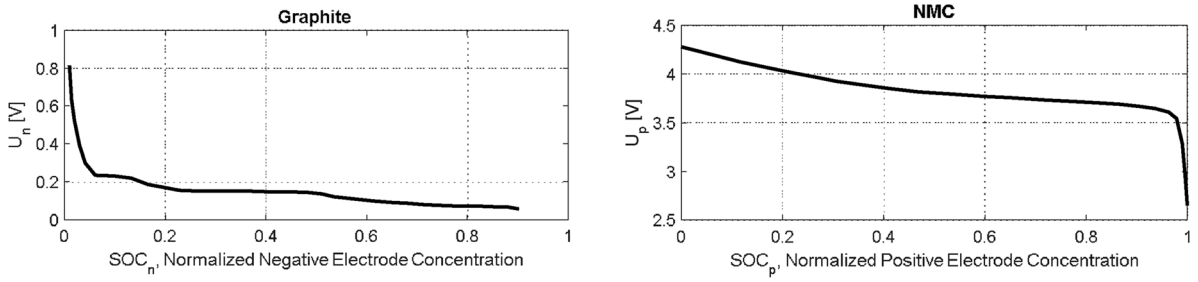

Fig. 6. Electrode OCPs for NMC and Graphite [46].

Table 3
The set of model parameters with their initial values for the discharge capacity test data.

Notations	Parameters	Initial Values
R_n	Negative Electrode Equivalent Particle Radius (μm)	5
R_p	Positive Electrode Equivalent Particle Radius (μm)	5
A_n	Negative Electrode Equivalent Active Surface Area (m^2)	2
A_p	Positive Electrode Equivalent Active Surface Area (m^2)	2
D_n	Negative Electrode Solid Phase Diffusion Coefficient, $*10^{-14}$(m^2/s)	2
D_p	Positive Electrode Solid Phase Diffusion Coefficient, $*10^{-14}$(m^2/s)	2
k_n	Negative Electrode Surface Reaction Rate Constant, $*10^{-11}$($m^{2.5}$/$mol^{0.5}$/ s)	2
k_p	Positive Electrode Surface Reaction Rate Constant, $*10^{-11}$($m^{2.5}$/$mol^{0.5}$/ s)	2
$c_{max,n}$	Negative Electrode Maximum Lithium ion Concentration (mol/m^3)	25000
$c_{max,p}$	Positive Electrode Maximum Lithium ion Concentration (mol/m^3)	22000
$SOC_{n,100}$	Negative Electrode SOC at Beginning-of-Discharge (BOD) after Full Charge	0.90
$SOC_{p,100}$	Positive Electrode SOC at Beginning-of-Discharge (BOD) after Full Charge	0.02
R_f	Cell Contact Resistance (Ω)	0.02
c_e	Solution Phase Concentration (mol/m^3)	1000

regarded as non-aging-related.

The parameter identification process is conducted in two steps. First, all parameters are identified from capacity test data from a fresh battery using the simplex search method aimed at minimizing the square errors between experimental and simulated voltage responses. In the second step, the non-aging-related parameters are regarded as constants, and the identification is run for the subset of parameters that are affected by aging using the MCMC algorithm. The aging-related parameters are identified as distributions.

The Bayesian methodology for parameter identification treats parameters as stochastic distributions rather than a constant. The essence of this approach lies in the Bayes' relation:

$$p(\theta|Data) = \frac{p(Data|\theta)p(\theta)}{p(Data)} = \frac{p(Data|\theta)p(\theta)}{\int p(Data|\theta)d\theta} \quad (17)$$

where the vector $\theta = [A_p, D_n, D_p, k_n, k_p, SOC_{n,BOD}, SOC_{p,BOD}]$ contains the aging-related parameter set in this study. $p(\theta)$ is the prior distribution of the parameter set, which quantifies the prior knowledge of θ ; $p(Data|\theta)$ is the likelihood distribution, which quantifies the probability of the observed voltage data given the parameter set θ ; $p(Data)$ is the normalizing constant, representing the probability of the observed voltage data; $p(\theta|Data)$ is the posterior distribution which quantifies the conditional probability distribution of the parameter set θ given the observed voltage data.

While the analytical solution of Eq. (17) is intractable, numerical sampling methodologies are desired for the approximation of probabilistic distribution $p(\theta|Data)$. The MCMC algorithm is one of the effective methodologies, and is applied according to following steps [47]:

Step 1: Set the number of sampling iterations N = 50,000 in this study.

Step 2: Start with initial values of the aging-related parameter set θ^0, which can be determined arbitrarily or from some preliminary results based on efficient optimization routines, such as the simplex search method. The latter is recommended because it can help the MCMC algorithm approximate its results more efficiently [47].

Step 3: Initialize aging-related variables for the implementation of the MCMC algorithm.

(1) The error variance of the initial fit is defined as:

$$err^2 = \frac{1}{n-p}\cdot SE_\theta$$

The n is the length of the time vectors, p is the length of the parameter set θ, the SE_θ is the square error between simulated and experimental voltage responses under certain parameter set θ:

$$SE_\theta = \sum_{j=1}^{n} [\mathbf{V}_{model,j}(\theta) - \mathbf{V}_{exp,j}]^2$$

The $\mathbf{V}_{model,j}$ and $\mathbf{V}_{exp,j}$ are the voltage outputs of the SP model and the experiment at each time instance j;

(2) Set $\mathbf{D} = 0.01\cdot\theta^0\cdot\mathbf{I}$ as the constant parameter walking distance for the following steps; θ^0 is the vector containing initial values of the aging-related parameter set.

I is the identity matrix of size 7 × 7, which is determined by the length of parameter set θ.

Step 4: Approximate the parameter distributions for N iterations

For i= 1, 2, ..., N

Generate a new candidate set of parameters in a random-walk manner:

$$\theta^* = \theta^{i-1} + \mathbf{D}z$$

where z is a random variable drawn from a normal distribution with zero mean value and standard deviation 1, Normal(0,1), to facilitate the random walk of the parameters;

Compute $SE_{\theta^*} = \sum_{j=1}^{n} [\mathbf{V}_{model,j}(\theta^*) - \mathbf{V}_{exp,j}]^2$;

Sample a random variable u from a uniform distribution, e.g. $u \in$ Uniform(0 1);

Compute $\alpha(\theta^*, \theta^{i-1}) = \min(1, e^{-\frac{[SE_{\theta^*} - SE_{\theta^{i-1}}]}{2err^2}})$;

If $u < \alpha(\theta^*, \theta^{i-1})$

Set $\theta^i = \theta^*$, $SE_{\theta^i} = SE_{\theta^*}$;

Else

Set $\theta^i = \theta^{i-1}$, $SE_{\theta^i} = SE_{\theta^{i-1}}$;

End

End

The traces of the seven aging-related parameters (A_p, D_n, D_p, k_n, k_p, $SOC_{n,100}$, $SOC_{p,100}$) over the 50,000 iteration window are displayed in Figs. 7(a)–(g). Generally speaking, it is common to identify a "Burn-in" period and a "Stable" period. The "Burn-in" period is the time window over which the parameter trace, after starting from an initial value, settles to its steady state. This phase is the transient phase for the identified parameter. In contrast, the "Stable" period is the time window over which the mean value of the parameter trace stays approximately constant. While the $SOC_{n,BOD}$ in Fig. 7(a) and the A_p in Fig. 7(b) quickly reach steady states, the k_p in Fig. 7(f) is the slowest one, taking nearly 30,000 iterations. The choice made in this work is to separate the 50,000 iterations into the initial "Burn-in" period, consisting of the first 30,000 iterations, and the "Stable" period related to the last 20,000 iterations. Information from the "burn-in" period should be discarded due to its transient nature, whereas the data in the "stable" period are used to obtain the estimate of the parameter distributions.

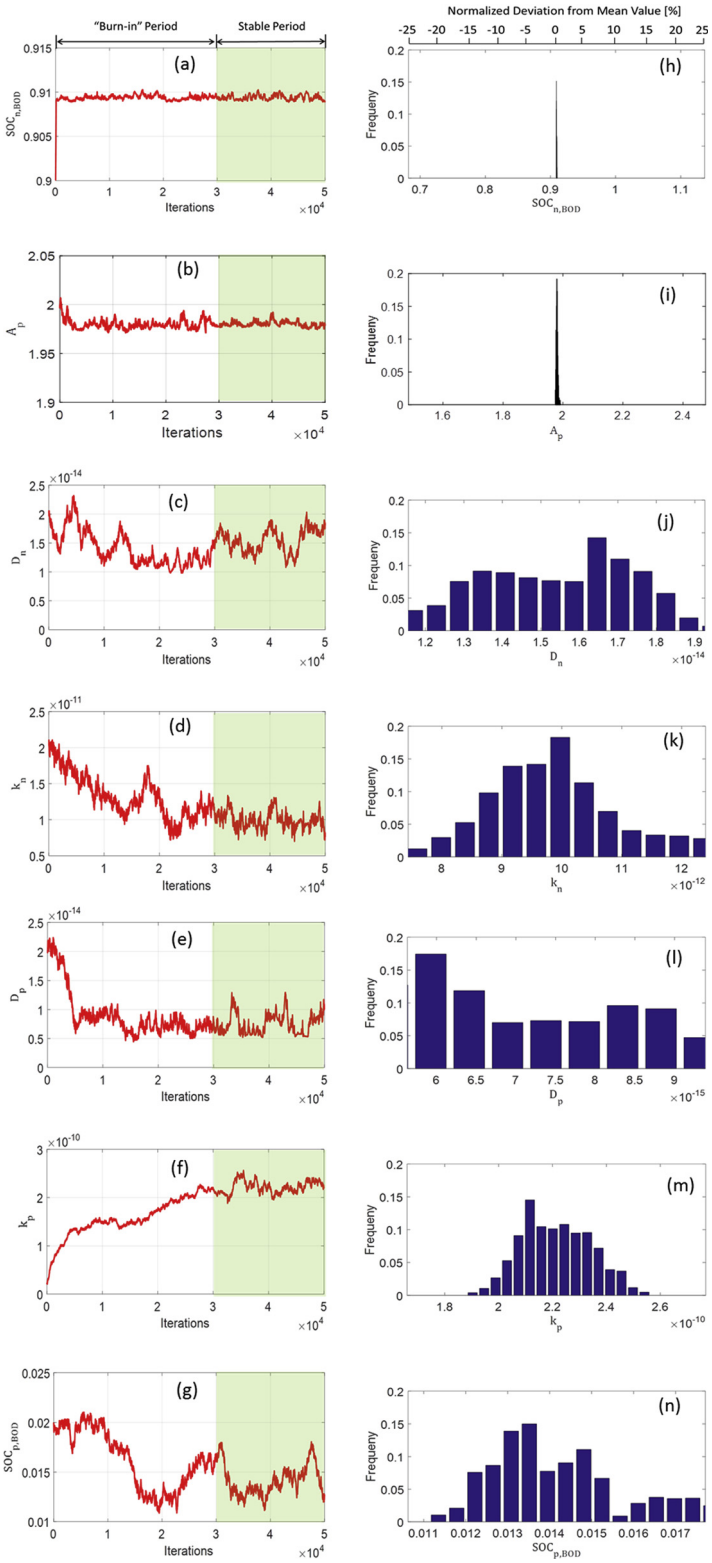

Fig. 7. The traces of aging-related parameters in the MCMC exploration with 50,000 iterations (a) – (g); the distributions of the aging-related parameters with the last 20,000 iterations of the parameter traces (h) – (n), which are all visualized in the [-25%, 25%] normalized deviation window around their mean values for comparison.

Figs. 7(h)–(n) show the parameter distributions for the SP model from the MCMC algorithm. The distributions of A_p, in Fig. 7(h), and $SOC_{n,100}$ in Fig. 7(i), vary in much narrower windows than the other parameters, which have rather wide variation windows, indicating high uncertainty of parameter identification. In other words, among the aging-related parameters, only A_p and $SOC_{n,100}$ can be identified with high confidence under the scenario of 1C discharge capacity test.

The cell capacity test data at different aging stages were fitted for cell #5 and #7 as examples in Fig. 8. Under both test scenarios with the same aging profile at two different temperatures (23 °C and 45 °C), the

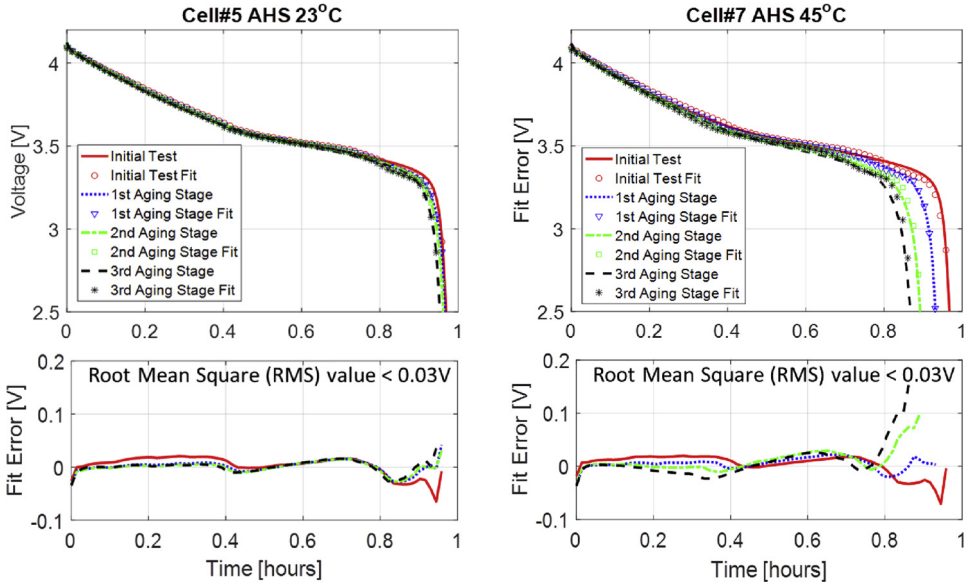

Fig. 8. Experimental and simulated 1C discharge data for the cell#5 under the AHS aging profile at 23°C and the cell#7 under the AHS aging profile at 45°C (top), and their corresponding fitting errors (bottom); the root mean square value of the fitting errors for both cases are under 0.03V.

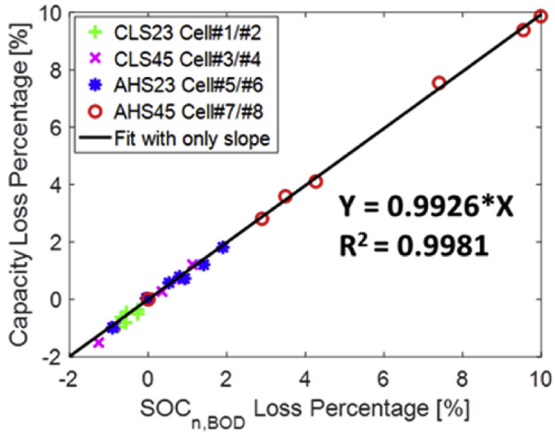

Fig. 9. Capacity loss vs. $SOC_{n,BOD}$ loss.

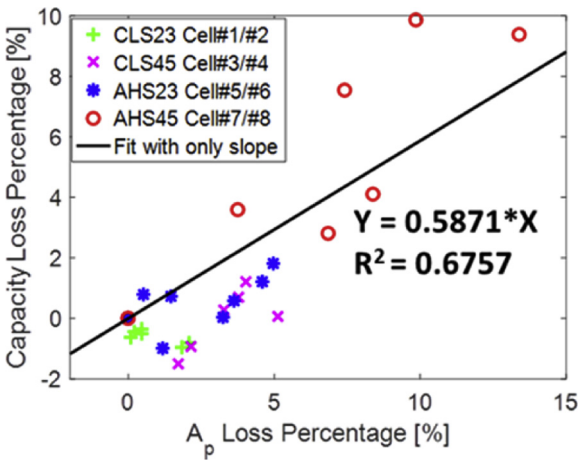

Fig. 10. Capacity loss vs. A_p loss.

root mean square (RMS) errors between experimental and simulated data were kept under 0.03 V, indicating satisfactory parameter identification performance. The A_p, which indicates the positive electrode active material loss, decreases in all cases. The $SOC_{n,100}$, which implies the active lithium ion loss and SEI growth, is overall reducing except in a few characterization stages. By correlating the variations of the two significant aging parameters with the capacity loss in Figs. 9 and 10, it is found that the loss of $SOC_{n,100}$ is strongly positively related to capacity loss ($R^2 = 0.9926$), yet the relationship between A_p loss and capacity loss is loose ($R^2 = 0.6757$). In the perspective of aging mechanisms, these correlations indicate that during the testing period used in this study, the degradation at the negative electrode (mainly SEI film growth) is the most significant cause of capacity loss; the degradation at the positive electrode affects the capacity loss in a limited manner.

5. Conclusions

This study aims to characterize the aging conditions of NMC lithium ion batteries for 48 V mild HEV application, which normally operates in a shallow SOC range and at high C rates. A set of in-house test profiles synthesized from real-world driving data were applied under different temperatures for accelerated cell aging testing. After the aging campaign, the capacity loss is much severer than the internal resistance rise and shows negative impacts from elevated temperature and higher discharge current rate. Further increasing the discharge current above a certain level does not result in a higher cell aging rate in terms of Ah-throughput, but can reduce testing time for the same amount of capacity loss. As the single-particle model is capable of simulating the battery voltage response under low current scenarios, its parameters are identified with the 1C discharge data at each aging characterization stage to imply potential aging mechanisms. Out of seven aging-related parameters, only two parameters can be identified with high confidence based on the Bayesian MCMC parameter identification algorithm. To identify other parameters, other test scenarios should be carried out to integrate more information into the identification process in future studies. The variation of negative electrode SOC after full charge, $SOC_{n,100}$, is found to strongly linearly correlate with the loss of cell capacity, suggesting the degradation at the negative electrode is the main aging mechanism in the 18650 NMC cell used in 48 V vehicle applications.

The findings from this research regarding the high correlation between the $SOC_{n,100}$ and the loss of cell capacity are specifically significant in that they can facilitate implementation of onboard battery capacity estimation and battery prognostics for micro-hybrid applications.

Acknowledgment

The authors would like to acknowledge Johnson Controls Power Solutions Group for their financial support. In particular, we would like to thank Mike Andrew for overseeing our collaboration and Dr. Zoe Jin for sharing her technical knowledge throughout the duration of the project. The help of Anirudh Allam with the experimental battery testing is also acknowledged.

References

[1] A. Dinger, R. Martin, X. Mosquet, M. Rabl, D. Rizoulis, M. Russo, G. Sticher, Batteries for Electric Cars: Challenges, Opportunities, and the Outlook to 2020 7 The Boston Consulting Group, 2010, p. 2017.
[2] J. Schmalstieg, S. Käbitz, M. Ecker, D.U. Sauer, A holistic aging model for Li (NiMnCo) O 2 based 18650 lithium-ion batteries, J. Power Sources 257 (2014) 325–334.
[3] M. Ecker, N. Nieto, S. Käbitz, J. Schmalstieg, H. Blanke, A. Warnecke, D.U. Sauer, Calendar and cycle life study of Li (NiMnCo) O 2-based 18650 lithium-ion batteries, J. Power Sources 248 (2014) 839–851.
[4] S.F. Schuster, T. Bach, E. Fleder, J. Müller, M. Brand, G. Sextl, A. Jossen, Nonlinear aging characteristics of lithium-ion cells under different operational conditions, J. Energy Storage 1 (2015) 44–53.
[5] A. Barré, B. Deguilhem, S. Grolleau, M. Gérard, F. Suard, D. Riu, A review on lithium-ion battery ageing mechanisms and estimations for automotive applications, J. Power Sources 241 (2013) 680–689.
[6] M. Ecker, J.B. Gerschler, J. Vogel, S. Käbitz, F. Hust, P. Dechent, D.U. Sauer, Development of a lifetime prediction model for lithium-ion batteries based on extended accelerated aging test data, J. Power Sources 215 (2012) 248–257.
[7] S. Käbitz, J.B. Gerschler, M. Ecker, Y. Yurdagel, B. Emmermacher, D. André, D.U. Sauer, Cycle and calendar life study of a graphite| LiNi 1/3 Mn 1/3 Co 1/3 O 2 Li-ion high energy system. Part A: full cell characterization, J. Power Sources 239 (2013) 572–583.
[8] W. Waag, S. Käbitz, D.U. Sauer, Experimental investigation of the lithium-ion battery impedance characteristic at various conditions and aging states and its influence on the application, Appl. Energy 102 (2013) 885–897.
[9] K. Amine, J. Liu, S. Kang, I. Belharouak, Y. Hyung, D. Vissers, G. Henriksen, Improved lithium manganese oxide spinel/graphite Li-ion cells for high-power applications, J. Power Sources 129 (1) (2004) 14–19.
[10] M.M. Joglekar, N. Ramakrishnan, Cyclic capacity fade plots for aging studies of Li-ion cells, J. Power Sources 230 (2013) 143–147.
[11] A. Cordoba-Arenas, S. Onori, Y. Guezennec, G. Rizzoni, Capacity and power fade cycle-life model for plug-in hybrid electric vehicle lithium-ion battery cells containing blended spinel and layered-oxide positive electrodes, J. Power Sources 278 (2015) 473–483.
[12] M. Dubarry, C. Truchot, M. Cugnet, B.Y. Liaw, K. Gering, S. Sazhin, C. Michelbacher, Evaluation of commercial lithium-ion cells based on composite positive electrode for plug-in hybrid electric vehicle applications. Part I: initial characterizations, J. Power Sources 196 (23) (2011) 10328–10335.
[13] M. Dubarry, C. Truchot, B.Y. Liaw, K. Gering, S. Sazhin, D. Jamison, C. Michelbacher, Evaluation of commercial lithium-ion cells based on composite positive electrode for plug-in hybrid electric vehicle applications. Part II. Degradation mechanism under 2C cycle aging, J. Power Sources 196 (23) (2011) 10336–10343.
[14] B. Stiaszny, J.C. Ziegler, E.E. Krauß, J.P. Schmidt, E. Ivers-Tiffée, Electrochemical characterization and post-mortem analysis of aged LiMn 2 O 4–Li (Ni 0.5 Mn 0.3 Co 0.2) O 2/graphite lithium ion batteries. Part I: cycle aging, J. Power Sources 251 (2014) 0439–0450.
[15] Y. Zhang, C.Y. Wang, X. Tang, Cycling degradation of an automotive LiFePO 4 lithium-ion battery, J. Power Sources 196 (3) (2011) 1513–1520.
[16] J. Wang, P. Liu, J. Hicks-Garner, E. Sherman, S. Soukiazian, M. Verbrugge, P. Finamore, Cycle-life model for graphite-LiFePO 4 cells, J. Power Sources 196 (8) (2011) 3942–3948.
[17] S. Onori, P. Spagnol, V. Marano, Y. Guezennec, G. Rizzoni, A new life estimation method for lithium-ion batteries in plug-in hybrid electric vehicles applications, Int. J. Power Electron. 4 (3) (2012) 302–319.
[18] D.I. Stroe, M. Świerczyński, A.I. Stan, R. Teodorescu, S.J. Andreasen, Accelerated lifetime testing methodology for lifetime estimation of lithium-ion batteries used in augmented wind power plants, IEEE Trans. Ind. Appl. 50 (6) (2014) 4006–4017.
[19] R.G. Jungst, G. Nagasubramanian, H.L. Case, B.Y. Liaw, A. Urbina, T.L. Paez, D.H. Doughty, Accelerated calendar and pulse life analysis of lithium-ion cells, J. Power Sources 119 (2003) 870–873.
[20] E.V. Thomas, H.L. Case, D.H. Doughty, R.G. Jungst, G. Nagasubramanian, E.P. Roth, Accelerated power degradation of Li-ion cells, J. Power Sources 124 (1) (2003) 254–260.
[21] M. Broussely, P. Biensan, F. Bonhomme, P. Blanchard, S. Herreyre, K. Nechev, R.J. Staniewicz, Main aging mechanisms in Li ion batteries, J. Power Sources 146 (1) (2005) 90–96.
[22] B. Stiaszny, J.C. Ziegler, E.E. Krauß, J.P. Schmidt, E. Ivers-Tiffée, Electrochemical characterization and post-mortem analysis of aged LiMn 2 O 4–Li (Ni 0.5 Mn 0.3 Co 0.2) O 2/graphite lithium ion batteries. Part I: cycle aging, J. Power Sources 251 (2014) 439–450.
[23] R.G. Jungst, G. Nagasubramanian, H.L. Case, B.Y. Liaw, A. Urbina, T.L. Paez, D.H. Doughty, Accelerated calendar and pulse life analysis of lithium-ion cells, J. Power Sources 119 (2003) 0870–0873.
[24] J.D. Kozlowski, Electrochemical cell prognostics using online impedance measurements and model-based data fusion techniques, Aerospace Conference, 2003. Proceedings 7 (2003) 3257–3270 (2003, March) IEEE, IEEE.
[25] M. Safari, M. Morcrette, A. Teyssot, C. Delacourt, Life prediction methods for lithium-ion batteries derived from a fatigue approach ii. Capacity-loss prediction of batteries subjected to complex current profiles, J. Electrochem. Soc. 157 (7) (2010) A892–A898.
[26] J. Wang, P. Liu, J. Hicks-Garner, E. Sherman, S. Soukiazian, M. Verbrugge, P. Finamore, Cycle-life model for graphite-LiFePO 4 cells, J. Power Sources 196 (8) (2011) 03942–03948.
[27] L. Serrao, S. Onori, G. Rizzoni, Y. Guezennec, "A novel model-based algorithm for battery prognosis,", Proceeding of the 7th IFAC Symposium on Fault Detection, Supervision and Safety of Technical Processes, (2009).
[28] X. Hu, S. Li, H. Peng, A comparative study of equivalent circuit models for Li-ion batteries, J. Power Sources 198 (2012) 359–367.
[29] G.K. Prasad, C.D. Rahn, Development of a first principles equivalent circuit model for a lithium ion battery, October), ASME 2012 5th Annual Dynamic Systems and Control Conference Joint With the JSME 2012 11th Motion and Vibration Conference (2012) 369–375.
[30] B. Saha, S. Poll, K. Goebel, J. Christophersen, An Integrated Approach to Battery Health Monitoring Using Bayesian Regression and State Estimation. In 2007 IEEE Autotestcon (September) IEEE, (2007), pp. 646–653.
[31] U. Tr ltzsch, O. Kanoun, H.R. Tränkler, Characterizing aging effects of lithium ion batteries by impedance spectroscopy, Electrochim. Acta 51 (8) (2006) 1664–1672.
[32] M. Doyle, T.F. Fuller, J. Newman, J. Electrochem. Soc. 140 (1526) (1993).
[33] G. Ning, B.N. Popov, Cycle life modeling of lithium-ion batteries, J. Electrochem. Soc. 151 (10) (2004) A1584–A1591.
[34] S. Santhanagopalan, Q. Guo, P. Ramadass, R.E. White, Review of models for predicting the cycling performance of lithium ion batteries, J. Power Sources 156 (2) (2006) 620–628.
[35] Q. Zhang, R.E. White, Capacity fade analysis of a lithium ion cell, J. Power Sources 179 (2) (2008) 793–798.
[36] J. Marcicki, F. Todeschini, S. Onori, M. Canova, Nonlinear parameter estimation for capacity fade in lithium-ion cells based on a reduced-order electrochemical model, 2012 American Control Conference (ACC), (2012), pp. 572–577 June IEEE.
[37] A.P. Schmidt, M. Bitzer, Á.W. Imre, L. Guzzella, Experiment-driven electrochemical modeling and systematic parameterization for a lithium-ion battery cell, J. Power Sources 195 (15) (2010) 5071–5080.
[38] M. Safari, M. Morcrette, A. Teyssot, C. Delacourt, Multimodal physics-based aging model for life prediction of Li-ion batteries, J. Electrochem. Soc. 156 (3) (2009) A145–A153.
[39] X. Lin, J. Park, L. Liu, Y. Lee, A.M. Sastry, W. Lu, A comprehensive capacity fade model and analysis for Li-ion batteries, J. Electrochem. Soc. 160 (10) (2013) A1701–A1710.
[40] J.C. Forman, S.J. Moura, J.L. Stein, H.K. Fathy, Genetic parameter identification of the doyle-fuller-newman model from experimental cycling of a lifepo 4 battery, American Control Conference (ACC), (2011), pp. 362–369 (2011, June)IEEE.
[41] V. Ramadesigan, K. Chen, N.A. Burns, V. Boovaragavan, R.D. Braatz, V.R. Subramanian, Parameter estimation and capacity fade analysis of lithium-ion batteries using reformulated models, J. Electrochem. Soc. 158 (9) (2011) A1048–A1054.
[42] R. Ahmed, J. Gazzarri, S. Onori, S. Habibi, R. Jackey, K. Rzemien, J. Tjong, J. LeSage, Model-based parameter identification of healthy and aged li-ion batteries for electric vehicles, SAE Int. J. Altern. Power 4 (2) (2015), https://doi.org/10.4271/2015-01-0252.
[43] P. Ramadass, B. Haran, P.M. Gomadam, R. White, B.N. Popov, Development of first principles capacity fade model for Li-ion cells, J. Electrochem. Soc. 151 (2) (2004) A196–A203.
[44] Z. Liu, A. Ivanco, Z.S. Filipi, Impacts of real-world driving and driver aggressiveness on fuel consumption of 48V mild hybrid vehicle, Sae Int. J. Altern. Powertrains 5 (2016) 2016-01-1166.
[45] Z. Liu, S. Onori, A. Ivanco, Synthesis and experimental validation of battery aging test profiles based on real-world duty cycles for 48V mild hybrid vehicles, IEEE Trans. Veh. Technol. (2017).
[46] V.R. Subramanian, V.D. Diwakar, D. Tapriyal, Efficient macro-micro scale coupled modeling of batteries, J. Electrochem. Soc. 152 (10) (2005) A2002–A2008.
[47] S.B. Chikkannanavar, D.M. Bernardi, L. Liu, A review of blended cathode materials for use in Li-ion batteries, J. Power Sources 248 (2014) 91–100.
[48] A. Solonen, Monte Carlo Methods in Parameter Estimation of Nonlinear Models, Master Thesis, Lappeenranta University of Technology, 2006.
[49] National Renewable Energy Laboratory, Transportation Secure Data Center, 2014, www.nrel.gov/tsdc.
[50] USABC electric vehicle Battery Test Procedures Manual. http://www.uscar.org/guest/article_view.php?articles_id=74.